

Propagation of Streamline Segment Length Distributions in a Wavy Channel Flow of Favorable and Adverse Pressure Gradients

Alexander Rubbert

Institute of Aerodynamics
RWTH Aachen University
Wüllnerstr. 5a, 52062 Aachen, Germany
a.rubbert@aia.rwth-aachen.de

Marian Albers

Institute of Aerodynamics
RWTH Aachen University
Wüllnerstr. 5a, 52062 Aachen, Germany
m.albers@aia.rwth-aachen.de

Michael Klaas

Institute of Aerodynamics
RWTH Aachen University
Wüllnerstr. 5a, 52062 Aachen, Germany
m.klaas@aia.rwth-aachen.de

Wolfgang Schröder

Institute of Aerodynamics
RWTH Aachen University
Wüllnerstr. 5a, 52062 Aachen, Germany
office@aia.rwth-aachen.de

ABSTRACT

Tomographic PIV measurements and DNS were conducted in a wavy channel flow to detect streamline segment statistics. Based on the data, the local streamline segment parameters were determined and the segment stretching mechanism was investigated in the frame of the model function proposed by Schäfer *et al.* (Schäfer *et al.* (2012a)). The model parameter a_∞ as defined by Schäfer *et al.* could be identified as the main influence on the stretching mechanism.

INTRODUCTION AND MOTIVATION

Turbulence has been in the focus of research in fluid mechanics for decades. While many approaches describe turbulence in terms of local point statistics, which has led to a wide range of turbulence models, no single model has proved to be universal. Each model has case-specific strengths and weaknesses and often requires an experienced user to fine-tune model parameters for each case, thus limiting its predictive quality and proving prone to errors. To improve the description of turbulent flows, Peters & Wang (2006) proposed the dissipation element method which decomposes a scalar flow field into an ensemble of spatially non-overlapping, monotonous sub-volumes - the dissipation elements - containing the geometric and topologic information of the instantaneous flow field. Further investigations using this method were performed experimentally (Schäfer *et al.* (2011), Schäfer *et al.* (2013)) as well as numerically (Wang & Peters (2008)) in a fully turbulent channel flow.

Wang (2010) proposed a variation of this method. Instead of considering volumetric structures of an arbitrarily selected scalar, streamlines are traced throughout the instantaneous flow field and divided into sections of monotonous absolute velocities. Unlike the dissipation element method, this method follows the inherent topology of the flow rather than imposing a mathematical formulation of a scalar. In extensive studies by Schäfer *et al.* (Schäfer *et al.* (2012a), Schäfer *et al.* (2012b)), a model function for the normalized streamline segment length distribution was derived for a multitude of homogeneous turbulence cases. It was found that the mean segment length is of the order on the Taylor microscale rather than the Kolmogorov length suggesting the potential to exploit this characteristic in future turbulence modeling approaches.

Previous investigations of wavy channel flows were able to show varying statistical behavior depending on the local mean flow conditions such as mean strain and pressure gradients

(Rubbert *et al.* (2017)), which significantly impact the statistical asymmetry between accelerating and decelerating segments in the investigated wavy channel flow. The scope of the current investigation is the analysis of the responsible stretching mechanism in the frame of the model function for streamline segment length distributions of favorable and adverse pressure gradients. To achieve this, tomographic PIV measurements and DNS computations were conducted in a wavy channel flow at $Re_{Bulk} = 3200$ and all required statistics were extracted.

MODEL FUNCTION

The model function for the propagation of the streamline segments length distribution $P(l)$ proposed by Schäfer *et al.* (2012a) is based on DNS studies of homogeneous isotropic decaying turbulence. It is formulated in the normalized quantities $\tilde{l} = l/l_m$ and $\tilde{P}(\tilde{l}) = l_m P(l/l_m)$. The normalization parameters include the mean streamline segment length l_m and the limit for large segments of inner streamline segment strain $a_\infty = (d\langle\Delta u|l\rangle/dl)|_{l\rightarrow\infty}$, which can be retrieved from segment statistics. The model function describes two types of processes driving the structure propagation. Stretching and contracting of structures occur continuously due to their inner velocity difference, which is further influenced when a structure passes through regions of a particular local strain and pressure gradients. Additionally, diffusive processes cause small structures to gradually disappear over time as their inner velocity difference diminishes. These continuous processes are modeled through the first and second order terms \tilde{a}_1 and \tilde{a}_2 summarizing drift, pressure, and diffusion based influences.

The remaining two contributions to the propagation equation are cutting and reattaching processes which occur nearly instantly when the iso-surface with a streamwise velocity gradient of zero moves perpendicular to the velocity into otherwise monotonous structures. These two fast processes are modeled by the cutting frequency Λ_c and the reattachment frequency Λ_a .

Consequently, the model function for the streamline segment length distribution as proposed by Schäfer *et al.* (2012a) is formulated as follows:

$$\begin{aligned}
\frac{d\tilde{P}(\tilde{l}, t)}{dt} + \frac{\partial}{\partial \tilde{l}} \left[\left(\tilde{a}_1(\tilde{l}) - \frac{\tilde{l}}{\tau_{l_m} a_\infty} \right) \tilde{P}(\tilde{l}, t) \right] \\
= \frac{1}{2} \frac{\partial^2}{\partial \tilde{l}^2} \left(\tilde{a}_2(\tilde{l}) \tilde{P}(\tilde{l}, t) \right) \\
+ \Lambda_c \left(2 \int_0^\infty \tilde{P}(\tilde{l} + \tilde{z}, t) d\tilde{z} - \tilde{P}(\tilde{l}, t) \right) \\
+ 2\Lambda_a \left(2 \int_0^{\tilde{l}} \frac{\tilde{z}}{\tilde{l}} \tilde{P}(\tilde{z}, t) \tilde{P}(\tilde{l} - \tilde{z}, t) d\tilde{z} - \tilde{P}(\tilde{l}, t) \right).
\end{aligned}$$

Note that unlike the exact formulation proposed by Schäfer, time is not non-dimensionalized by a_∞ since under the given flow conditions, near-zero or negative values can occur. Further analysis of the underlying processes lead to algebraic expressions for the term \tilde{a}_1 .

$$\tilde{a}_1 = \langle \Delta \tilde{u} | \tilde{l} \rangle + \tilde{v}_D + \tilde{v}_p.$$

To recognize that the mean segment length used for normalization can change over time, the model function expresses this by the time scale τ_{l_m} . In the current study, its value can be set to infinity since the statistics are locally normalized by the steady value for l_m rendering the term describing the renormalization unnecessary. While the conditional mean velocity difference $\langle \Delta \tilde{u} | \tilde{l} \rangle$ and the normalized segment flux $\frac{d\tilde{P}(\tilde{l}, t)}{dt}$ can be obtained from segment statistics, the values of \tilde{v}_D , \tilde{v}_p , Λ_c , and Λ_a are not immediately accessible. However, this allows for the separate consideration of stretching related phenomena and remaining contributions.

FACILITIES

All experiments were conducted in an Eiffel-type wind tunnel that provides a fully turbulent two-dimensional channel flow matching DNS results of Moser *et al.* (1999) in the test section which was verified in previous studies by Schäfer *et al.* (2011). This test section shown in figure 1 has an aspect ratio of 1:20 and measures $2 h \times w = 100 \text{ mm} \times 2,000 \text{ mm}$ (height \times width) at a test section length of $l = 2,500 \text{ mm}$, i.e., $50 h$ with the channel half-height h . The test section itself provides full optical access and is attached to a nine meter long inlet section (180 h) with two strips of sandpaper on its upstream end to enforce laminar-turbulent transition. The test section is equipped with exchangeable sidewalls allowing different flow conditions. In the current study, a sidewall with sinusoidal shape, a wavelength of 100 mm, and an amplitude of 5 mm was investigated for a bulk Reynolds number of 3200 based on the bulk streamwise velocity u_{Bulk} and the flat channel half height h . The trough of the wave is aligned with the previously flat surface such that the waves crests reach 10 mm into the flow. Due to the waviness of the sidewall, locally adverse pressure gradient (APG) and favorable pressure gradient (FPG) flow conditions occur in the channel.

To improve the local resolution of the streamline segment statistics and therefore to better correlate the results with the instantaneous flow state, the experimental setup consisting of four LaVision Imager sCMOS cameras and a New Wave Solo 200 XT Nd:YAG dual cavity laser was modified compared to previous studies Rubbert *et al.* (2017), in which four narrow cuboid volumes along the wave were illuminated by an incoming beam from the top of the channel and recorded separately without acquiring data from the surroundings. The modified setup provides a thick light sheet which is arranged perpendicular to the wavy channel surface allowing for a more detailed analysis of the streamline segment statistics

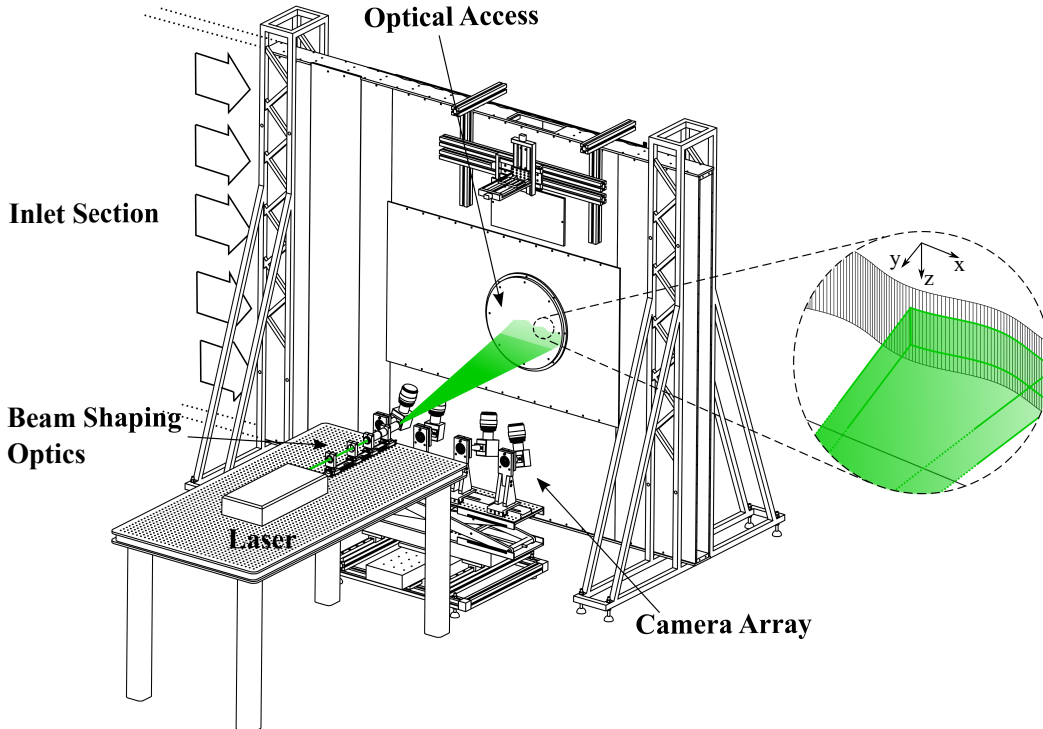


Figure 1. Measurement section and tomographic PIV setup; the enlargement shows the wavy sidewall.

by capturing a wider range of wall-normal distances and a larger section of the wave. The field of view was set to capture the surroundings of the wave, where effects of the decelerating flow, i.e., separation onset, and accelerating flow, in other word adverse and favorable pressure gradients, were expected.

COMPUTATIONAL SETUP

The dimensions of the physical domain are $L_x = 8h$, $L_y = 2h$, and $L_z = 4h$ in the streamwise, wall-normal, and spanwise direction. The wavy surface of the lower wall of the channel has a wave length of $\lambda = 2h$ such that four waves are included within the streamwise direction. At the wall, a grid resolution in inner wall units of $\Delta_x^+ = 4.1$, $\Delta_y^+ = 1.0$, and $\Delta_z^+ = 8.2$ is used, with a relaxation of the y -component towards the centerline of the channel. This yields a grid with $n_{cells} = 400 \times 120 \times 100 = 4.8 \cdot 10^6$ cells. Due to the sufficiently high resolution, the compressible unsteady Navier-Stokes equation is solved directly (DNS) on body-fitted grids. For the convective fluxes the advection upstream splitting method (AUSM) is used and a central scheme is employed for the viscous terms. The temporal integration is performed by an explicit 5-stage Runge-Kutta method at second-order accuracy. Investigations by Meinke *et al.* (2002) have shown the high quality of the results of this numerical method.

DATA PROCESSING

Using the velocity fields streamlines were traced starting from 10 000 homogeneously distributed seed points per snapshot. A 4-stage Runge-Kutta scheme was used for the spatial integration while the space step was set to one fifth of the local cell size. Local velocities between the grid points were determined using cubic spatial interpolation. Consequently, the local coordinate along each streamline and the absolute velocity were calculated from the spatial coordinates and local velocities of all contributing vertices resulting in two vectors. Local extrema were identified as vertices which have neighbors with larger or smaller absolute velocities. The streamline coordinate of such vertices was refined by fitting a parabola onto its own and its neighbor velocities and by determining the analytical location of its extremum. All other vertices were discarded. A streamline segment is defined by two neighboring extrema. Its arclength is the difference in the streamline coordinates while its characteristic velocity value is the difference between the velocity values at both constituting extrema.

Local statistics are determined based on a grid of 66 by 201 nodes. Each node is associated with all segments passing by within a distance of one grid space. By this approach, local statistics represent all structures which encompass the local node. Based on these statistics, structure fluxes and normalization parameters l_m and a_∞ are determined which are used to normalize the local statistics.

RESULTS AND DISCUSSION

First, the basic velocity statistics from DNS and experimental data were compared yielding satisfying agreement as shown in figure 2. The mean velocities present good agreement even though the DNS inherently produces smoother velocity distributions. Good agreement is also found in the fluctuation RMS statistics. The regions with high values for u'_{rms} trailing the crest and v'_{rms} in the trough region are clearly visible in both datasets and compares well in shape and magnitude. The experimental data does show some artifact near the wave surface, however.

Since the local mean streamwise velocity gradient was identified to impact the streamline segment statistics in terms of the ratio between mean segment length of positive and negative segments as well as the inner velocity difference, it was also used as a reference to analyze segment stretching phenomena. Its distribution is presented in figure 3. The red lines represent streamlines based on the

mean velocity field to visualize the location and extent of the separation bubble. Due to the separation, the local streamwise velocity gradient distribution does not follow the wall contour. The flow decelerates moderately until well after the wave's trough. When it reaches the contraction slope of the wave the flow accelerates due to the geometric convergence of the channel.

Within the separated region, very large locally confined acceleration and deceleration regions exist due to the high rate of change of the flow direction. This region is of particular interest when the impact of the mean velocity gradient on stretching behavior is analyzed.

Schäfer *et al.* (2012a) propose an algebraic approximation for the conditional mean inner velocity differences of streamline segments

$$\langle \Delta \tilde{u} | \tilde{l} \rangle \approx \alpha_u \frac{\tilde{l}^\beta}{\beta_u + \tilde{l}^\beta}.$$

This term approximates the mean velocity difference with all streamline segments of the given length \tilde{l} . This notation serves to show that its contribution to the overall segment behavior due to stretching asymptotically converges to a linear relation in the long segment limit. Schäfer *et al.* (2012a) propose model constants of $\alpha_u = 1$ and $\beta_u = 6$ which due to the normalization correspond to a_∞ and $6a_\infty$ in the current notation since the temporal normalization with a_∞ was omitted. Therefore, the paramount importance of the stretching behavior in the large segment limit for all other scales is evidenced through this expression. Intuitively, it can be argued that a_∞ should assume the value of the streamwise velocity gradient since the velocity fluctuations along a streamline have finite values such that in the limit of infinitely long segments they will be dominated by the velocity difference over the length of the segment and the mean velocity gradient.

However, the values for a_∞ obtained from the segment statistics in figure 4 do not match the local mean velocity gradient exactly. While some features of structure of the a_∞ -distribution resemble the mean velocity gradient and encompasses the same range of occurring values in regions of moderate acceleration such as the band of negative values spanning from $x/h = 0$ to 1 at $y/h \approx 0.2$ and the positive region above the contracting wall especially the pronounced acceleration regions in the separation are not present in a_∞ . Instead, it appears to be smoothed compared to the local velocity. Particularly noteworthy is the fact that the trough and separation region where a_∞ and dv_{abs}/ds differ most was already found to deviate from an otherwise generally good scaling of the streamline segment statistics asymmetry with dv_{abs}/ds (Rubbert *et al.* (2017)). The stretching mechanisms responsible for this scaling appears to be impeded in the trough and separation region. A possible reason for the deviation of the smoothed out a_∞ -distribution from the dv_{abs}/ds distribution might be the inability of the flow to immediately adjust to the local flow conditions. This argument is supported by the fact that both distributions match each other quite well in larger homogeneous regions with low spatial gradients while the structures cannot adapt to the abrupt change between acceleration and deceleration in the separation bubble.

Besides the stretching mechanism, which appears to be closely related to the mean velocity gradient, other contributions also affect the streamline length distribution. To approximate the local importance of the stretching mechanism, the propagation equation can be rewritten in a more compact form

$$\frac{d\tilde{P}(\tilde{l}, t)}{dt} + \frac{\partial}{\partial \tilde{l}} \left(\langle \Delta \tilde{u} | \tilde{l} \rangle \tilde{P}(\tilde{l}, t) \right) = R.$$

In this notation, all but the stretching contribution to the local

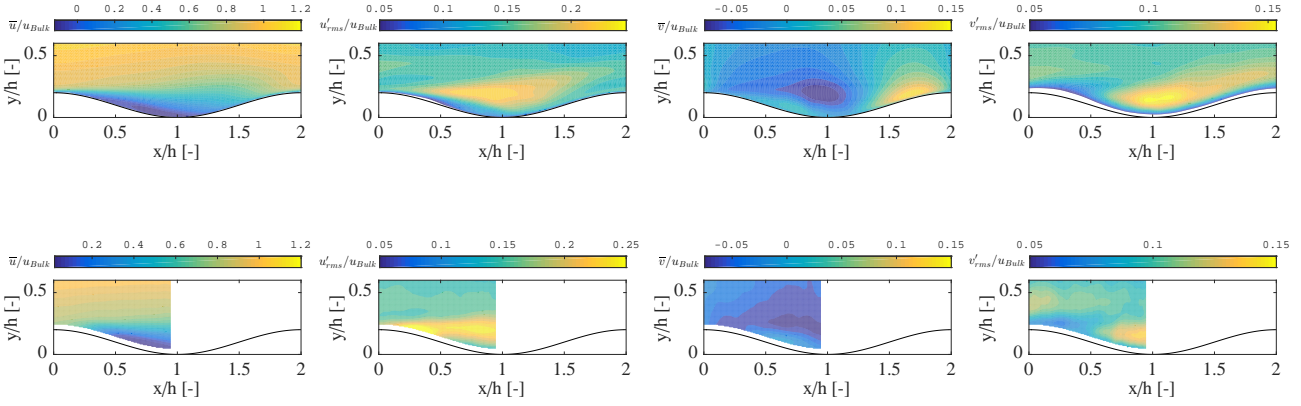


Figure 2. From left to right: $\bar{u}, u'_{rms}, \bar{v}, v'_{rms}$ for DNS (top) and experiment (bottom).

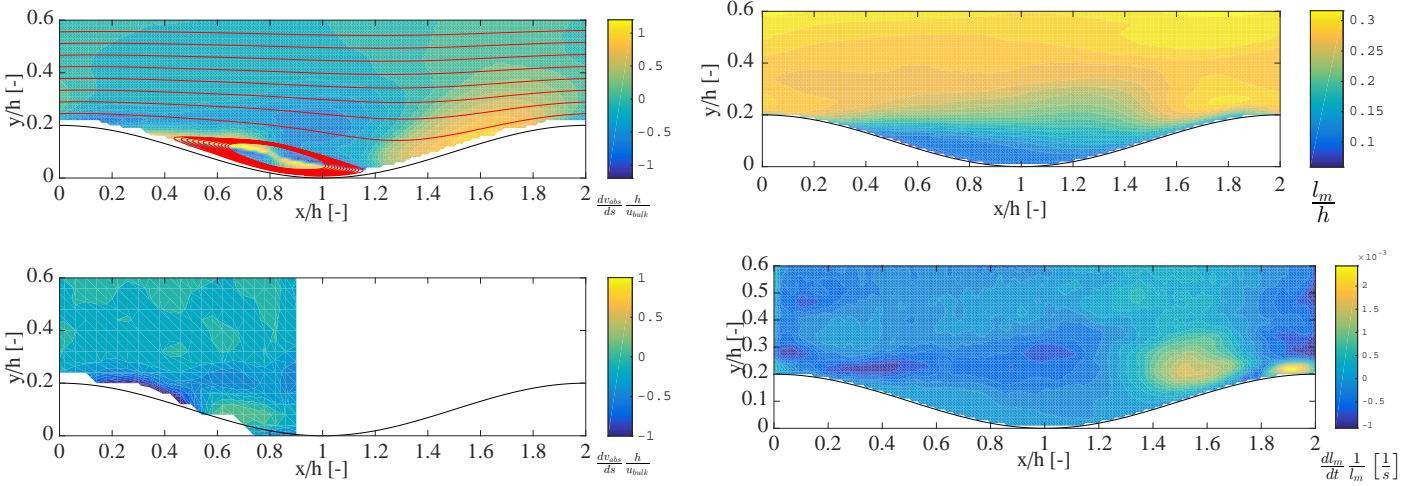


Figure 3. Local mean streamwise velocity gradient $\frac{dv_{abs}}{ds}$.

Figure 5. l_m (top) and its local convective change $\frac{dl_m}{dt}|_{total}$ (bottom) from DNS data.

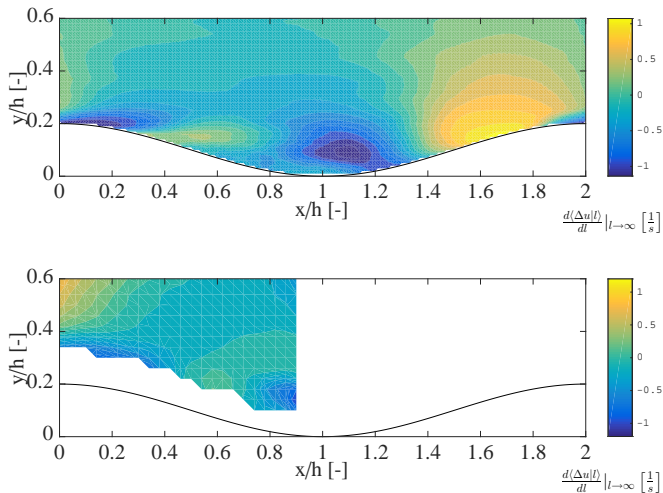


Figure 4. a_∞ from DNS (top) and experimental (bottom) data.

convective change in the segment length distribution are expressed in the residual term R . This is beneficial since all other terms are available from the streamline segmentation statistics. To better visualize the overall impact on the segment length distribution, the impact on the mean segment length l_m is considered instead of the change of $\tilde{P}(\tilde{l}, t)$.

$$\begin{aligned}
 l_m &= \int_0^\infty l P(l) dl \\
 \Rightarrow \frac{dl_m}{dt} &= \int_0^\infty l \frac{dP(l)}{dt} dl \int_0^\infty P(l) dl \\
 &= l_m \int_0^\infty \tilde{l} \frac{d\tilde{P}(\tilde{l})}{dt} d\tilde{l}
 \end{aligned}$$

The mean segment length and its resulting rate of change is shown in figure 5. After a relatively fast decrease in mean segment length at the separation onset at $[x/h, y/h] \approx [0.3, 0.2]$, the structure size decreases slowly while passing over the separation

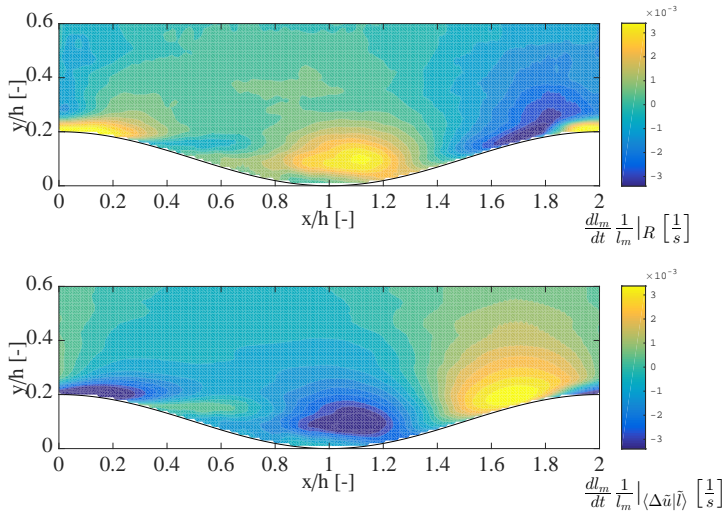


Figure 6. Contribution of the non-stretching term $\frac{dl_m}{dt}|_R$ (top) and stretching-based term $\frac{dl_m}{dt}|_{(\Delta\tilde{u}|\tilde{l})}$ (bottom) to the local change in mean structure size.

bubble before undergoing a faster segment length decrease at $[x/h, y/h] \approx [1, 0.3]$. The decrease in mean segment length is recovered when the flow accelerates over the contracting slope at $[x/h, y/h] \approx [1.5, 0.25]$, which roughly resembles the mean streamwise velocity gradient distribution in figure 3.

In close proximity to the wall and in the trough region, the structure of the convective rate of change of the mean structure size deviates significantly from the distribution of the local streamwise velocity gradient in figure 3. While there are multiple distinct peaks in the velocity gradient at $x/h = [0.4, 1.2]$, the change in the mean structure size is approximately zero. Over the contracting slope between $x/h = 1.2$ and $x/h = 1.8$, the region of significant flow acceleration extends to the wall. At the same time, the structure growth in close proximity to the wall remains almost zero and only shows a significant growth region at $y/h = 0.2$, which is approximately 0.1 above the wall surface.

To gain further insight into the streamline segment behavior, two separate contributions to the change in mean segment length were defined as

$$\frac{dl_m}{dt}|_R = l_m \int_0^\infty \tilde{l} R d\tilde{l} \quad \text{and}$$

$$\frac{dl_m}{dt}|_{(\Delta\tilde{u}|\tilde{l})} = l_m \int_0^\infty \tilde{l} \frac{\partial}{\partial \tilde{l}} (\langle \Delta\tilde{u}|\tilde{l} \rangle \tilde{P}(\tilde{l}, t)) d\tilde{l}.$$

They are shown in figure 6. It is immediately apparent that in the near wall region, the two mechanisms counteract each other explaining the near-zero impact of the high accelerations. Additionally, it is noteworthy that the stretching mechanism alone presents comparable magnitudes to the contribution of all remaining mechanisms. Finally, the distribution of stretching impact to the change in structure size is almost indistinguishable from the distribution of a_∞ in figure 4. Due to the fact that this term was obtained from the structure statistics without assuming Schäfer et al.'s algebraic approximation, it seems to confirm that the stretching moment is largely defined by the large scale parameter a_∞ .

CONCLUSION

Streamline segment statistics were experimentally and numerically investigated in wavy channel flow at $Re_{Bulk} = 3200$. The statistics were analyzed in terms of the model equation for segment length propagation by Schäfer et al. (Schäfer et al. (2012a)). First, the relation between the statistical parameter a_∞ and the local mean streamwise velocity gradient was theoretically reviewed which implied that both terms should converge. While the statistics closely resemble each other they are not the same, however. A possible reason for the deviation might be a required relaxation length of transported structure packets with a certain parameter to adjust to the local flow condition. This is further evidenced by the appearance of the a_∞ -distribution which lacks the small scale fidelity of the mean velocity gradient. Additionally, the propagation of the mean structure length was observed and split into a stretching contribution and a remaining term representing all other phenomena. Since stretching term's magnitude is largely comparable to the remaining contribution it is related to the major mechanism. Also, its close relation to a_∞ was shown which matches an algebraic approximation found in the model function. As a_∞ is a large scale quantity which still significantly contributes to the turbulent structure behavior, future work will be focused on achieving a prediction of this parameter based on other mean or large scale quantities which would represent a first step towards modeling the turbulent flow.

ACKNOWLEDGEMENT

This work was funded by the Deutsche Forschungsgesellschaft within the research project SCHR 309/41-2: Geometric Structure of Small Scale Turbulence.

REFERENCES

- Meinke, M., Schröder, W., Krause, E. & Rister, Th. 2002 A comparison of second- and sixth-order methods for large-eddy simulations. *Computers & Fluids* **31** (4), 695–718.
- Moser, R., Kim, J. & Mansour, N. 1999 Direct numerical simulation of turbulent channel flow up to $re_\tau = 590$. *Physics of Fluids* **11** (4), 943–945.
- Peters, N. & Wang, L. 2006 Dissipation element analysis of scalar fields in turbulence. *Comptes Rendus Mécanique* **334** (8-9), 493–506.
- Rubbert, A., Hennig, F., Klaas, M., Pitsch, H., Schröder, W. & Peters, N. 2017 Streamline segment scaling behavior in a turbulent wavy channel flow. *Experiments in Fluids* **58** (2), 10.
- Schäfer, L., Dierksheide, U., Klaas, M. & Schröder, W. 2011 Investigation of dissipation elements in a fully developed turbulent channel flow by tomographic particle-image velocimetry. *Physics of Fluids* **23** (3), 035106.
- Schäfer, L., Göbbert, J. H. & Schröder, W. 2013 Dissipation element analysis in experimental and numerical shear flow. *European Journal of Mechanics - B/Fluids* **38**, 85–92.
- Schäfer, P., Gampert, M. & Peters, N. 2012a The length distribution of streamline segments in homogeneous isotropic decaying turbulence. *Physics of Fluids* **24** (4), 045104.
- Schäfer, P., Gampert, M. & Peters, N. 2012b On the scaling of the mean length of streamline segments in various turbulent flows. *Comptes Rendus Mécanique* **340** (1112), 859–866, out of Equilibrium Dynamics.
- Wang, L. 2010 On properties of fluid turbulence along streamlines. *Journal of Fluid Mechanics* **648**, 183–203.
- Wang, L. & Peters, N. 2008 Length-scale distribution functions and conditional means for various fields in turbulence. *Journal of Fluid Mechanics* **608** (1), 113–138.